Constraining the Thickness of the Conductive Portion Europa's Ice Shell Using Sparse Radar Echoes

Dustin M. Schroeder [1,2], Natalie S. Wolfenbarger [1], Gregor B. Steinbrügge [3], Riley Culberg [4], Samuel M. Howell [3], Elizabeth Spiers [5], Marshall Styczinski [6]

[1]Department of Geophysics, Stanford University
[2]Department of Electrical Engineering, Stanford University
[3]Jet Propulsion Laboratory, California Institute of Technology
[4]Department of Earth and Atmospheric Sciences, Cornell University
[5]University of Texas Institute for Geophysics
[6]Blue Marble Space Institute of Science

Key Points:

- Radar-detectable interfaces from the subsurface of Europa's ice shell can be thermally diagnostic.
- The thickness of the conductive portion of Europa's ice shell can be constrained without direct detection of the ice–ocean interface.
- The detection of sparse echoes places a lower bound on conductive ice shell thickness based on the two-way integrated radar attenuation.

Corresponding author: Dustin Schroeder, `dustin.m.schroeder@stanford.edu`

Abstract

Ice-penetrating radar sounding is the primary geophysical technique for imaging the subsurface of planetary ice shells and has the potential to directly detect the ice–ocean interface. However, many sounding measurements may lack extensive features that would aid their physical interpretation. In this scenario, the detection of sparse echoes can also provide rich information on ice shell properties. To explore and demonstrate this possibility, we consider three cases of isolated radar signatures: pore-curing, eutectic melt, and unattributed echoes. We show that through detection of unattributed sparse echoes, the thickness of the conductive portion of Europa's ice shell can be constrained. These constraints can be improved by attributing sparse echoes to thermally-diagnostic signatures such as pore-curing and eutectic melt. Notably, this approach to radar sounding echo analysis is particularly compatible with joint inversions with other planetary geophysical observations such as tidal deformation, magnetic induction, and rotation state.

1 Introduction

Europa, Jupiter's fourth largest moon, is thought to host a young, dynamic ice shell and a global subsurface ocean (Pappalardo et al., 2024). Despite well-established observational and modeling evidence supporting this large-scale configuration, fundamental "open questions" remain about the moon's interior structure and processes (Roberts et al., 2023). Perhaps most salient among these are whether the ice shell is "thin" (kilometers) and thermally conductive from the surface to the ocean or whether it is "thick" (tens of kilometers) and includes a thermally conductive lid overlying a thermally-driven convecting layer (Billings & Kattenhorn, 2005; Roberts et al., 2023). The question of shell thickness and thermal structure is fundamental to the investigation of the Europa's formation, behavior, and evolution. Ice shell thickness and thermal structure are also critical for understanding how dynamic subsurface processes drive the formation of the surface features we can observe in surface imagery and topography (Daubar et al., 2024). These subsurface processes govern the exchange of material between the ocean and surface, critical to the moon's potential habitability (Vance et al., 2023; Becker et al., 2024). The scientific potential of NASA's Europa Clipper mission will rely on the development and refinement of observational approaches to constrain not only the total thickness of Europa's ice shell, but also the portion of the shell that is thermally conductive vs. convective (Pappalardo et al., 2024).

In terms of exploring the interior structure of icy moons and planetary bodies, classic geophysical investigations on planetary missions (e.g. gravity, magnetic induction, and rotation state) place constraints on models of their interiors (Roberts et al., 2023). For example, magnetometer observations can place limits on a combination of possible ice shell thickness and ocean conductivity/salinity (Roberts et al., 2023). In fact, this kind of magnetic-induction-based constraint using data from NASA's Galileo mission is the basis of our belief that Europa hosts a global subsurface ocean (Kivelson et al., 2000). Similarly, measurements of Europa's gravitational field—its static configurations and time-varying tidal signature—and global shape can limit the range of interior models compatible with observations, including ice shell thickness and thermophysical structure (Roberts et al., 2023). For these geodetic inversions, sources of non-uniqueness include the rheologic properties of the moon's ice shell, its porosity and grain size, and the deeper (non-water) structure of the moon (Roberts et al., 2023). Current approaches to strengthening these geodetic constraints involve improving the observations of tidal deformation, orbit determination, measurements of global and local shape, and the feasibility of observing librations (Mazarico et al., 2023a). Any additions to this portfolio of interior-sensitive geophysical observations have the potential to reduce the non-uniqueness of our inversions and enhance our constraints on properties of Europa's ice shell and ocean, including the layer thicknesses, which is a "Level-1" science goal for the Europa Clipper mission (Pappalardo et al., 2024).

In addition to the geophysical investigations described above, the Europa Clipper mission includes the Radar for Europa Assessment and Sounding: Ocean to Near-surface (REASON), which is an ice-penetrating radar sounder operating at 60 MHz and 9 MHz (Blankenship et al., 2024). The most powerful, complementary, and straightforward observation that REASON could add to magnetic and geodetic measurements would be direct detection of Europa's ice–ocean interface (Blankenship et al., 2024). Radar-sounding measurement of the depth to ice–ocean interface (or something very close to it) would provide a total ice shell thickness and enable the use of complementary magnetic or gravity data to estimate ocean thickness and salinity or other ice shell properties (temperature, rheology, etc.).

Depending on ice shell thickness, thermophysical structure, and chemistry, mapping the ice–ocean interface across all mission profiles and regions of the moon may or may not be possible (Kalousová et al., 2017; Blankenship et al., 2024). However, there are other features within the ice shell with the potential to produce signatures in radar sounding data which may be easier to detect because of their shallower depths and resulting lower integrated two-way attenuation losses (Blankenship et al., 2024). These features include both thermally-diagnostic features (like eutectic melt and the signature of pore curing) and more general attenuation-constraining signatures like isolated unattributed echoes (Schmidt et al., 2011; Kalousová et al., 2017; Culha et al., 2020; Steinbrügge et al., 2020; Culberg et al., 2021; Wolfenbarger et al., 2022; Souček et al., 2023). In this work, we explore how those signatures can be exploited as interior-constraining geophysical observations that complement magnetic and geodetic investigations by limiting the range of possible thicknesses for the conductive layer of Europa's ice shell.

2 Methods

To evaluate the potential for various radar signatures within Europa's ice shell (beyond echoes from the ice–ocean interface) to constrain the thickness of its thermally conductive layer, D_{cond}, we explore scenarios in which we assume such a given signature was observed and then illustrate the limit it places on D_{cond}. Essential to our approach is the recognition that many potential radar-detectable interfaces within Europa's ice shell are thermally diagnostic—their existence implies a temperature or range of temperatures at that depth. As such, to illustrate the character of constraints on D_{cond} placed by potential future radar observations, we must assume a thermal profile in depth. Following a similar approach by Howell (2021), we forward model a collection of ice shell thermal profiles. We adopt the thermal model of Chyba et al. (1998) given by

$$T(z) = T_s \exp\{z/h\}, \tag{1}$$

where $h = D_{\text{cond}}/\ln(T_{\text{conv}}/T_s)$, T_s is the surface temperature, and T_{conv} is the basal temperature assumed to be equal to the isothermal temperature of the convective layer. Note that the model of Chyba et al. (1998) is in a different form but mathematically equivalent to models considered in previous studies of Europa's ice shell (e.g., Howell, 2021; Johnson et al., 2017; Nimmo et al., 2003). We consider a range of T_s from 97−111 K, following the mean surface temperature range considered by Howell (2021) (104 ± 7 K in their Table 2). We vary D_{cond} from 3−50 km, but hold T_{conv} constant at 273 K, which represents the maximum temperature where ice is thermodynamically stable for this range of conductive layer thickness. Note that the approach we illustrate is generic and—once data are collected—can be used with more sophisticated thermal models and a larger family of profiles representing variations of all model parameters.

Because ice is a low-loss material at the frequencies relevant to this study (9 and 60 MHz), the attenuation rate α can be approximated in dB/m as

$$\alpha \approx 0.0009\sigma, \tag{2}$$

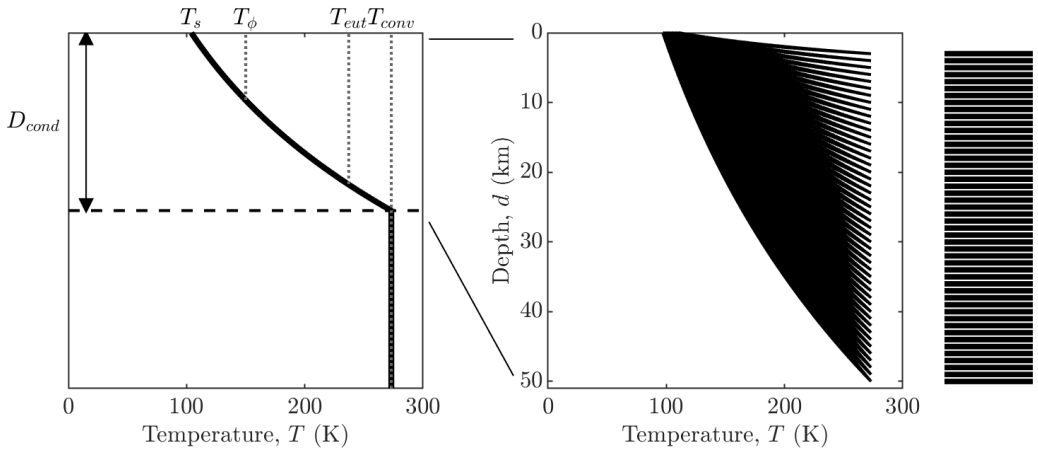

Figure 1. (left) An example of the ice shell thermal profile considered in this study and (right) a set of conductive-layer profiles resulting from a sweep of ice shell thickness and surface temperature. The black bars on the far right are a histogram representing a uniform distribution of conductive-layer thicknesses, where the length of the bar shows the number of profiles compatible with a given $D_{\rm cond}$. The parameters in this model include $D_{\rm cond}$, the thickness of the conductive layer, T_s, the surface temperature, T_ϕ, the porosity-curing temperature, $T_{\rm eut}$ the eutectic temperature, and $T_{\rm conv}$ the isothermal temperature of the convecting layer.

where σ is the electrical conductivity of the ice in µS/m (Moore, 2000). The electrical conductivity depends on both ice temperature and on the type and concentration of lattice-soluble impurities (e.g., F^-, Cl^-, $NH_4{}^+$, H^+) (Moore, 2000). We follow Moore (2000) and Souček et al. (2023) and assume chloride is the only lattice-soluble impurity in Europa's ice shell and therefore the electrical conductivity can be represented as

$$\sigma = \sigma_{\rm ice} \exp\left\{\frac{E_{\rm ice}}{k}\left(\frac{1}{T_r} - \frac{1}{T}\right)\right\} + \mu_{\rm Cl^-}[\rm Cl^-] \exp\left\{\frac{E_{\rm Cl^-}}{k}\left(\frac{1}{T_r} - \frac{1}{T}\right)\right\}, \tag{3}$$

where $\sigma_{\rm ice}$ is the electrical conductivity of pure ice, $E_{\rm ice}$ is the activation energy of pure ice, $\mu_{\rm Cl^-}$ is the molar conductivity of chlorides, $[\rm Cl^-]$ is the concentration of chloride in the ice, $E_{\rm Cl^-}$ is the activation energy of chlorides, k is the Boltzmann constant, T_r is the reference temperature at which the electrical properties were measured, T is the ice temperature. We follow Souček et al. (2023) and assume the mean values for these parameters as presented in Table 1 of MacGregor et al. (2007). Following MacGregor et al. (2015), the two-way attenuation to the base of the conductive lid, corresponding to a depth of $D_{\rm cond}$, can be represented as

$$A_2 = 2\int_0^{D_{\rm cond}} \alpha(z) dz\,, \tag{4}$$

where $\alpha(z)$ is the attenuation rate at a depth z (Equation 2).

Figure 2 shows the resulting illustrative family of temperature and chemistry-dependent attenuation rates predicted by the model used in this study. However, as with the thermal model, the approach we illustrate here is fully compatible with other attenuation models that either assume different dielectric parameters or do not employ the low-loss approximation when analyzing actual observations.

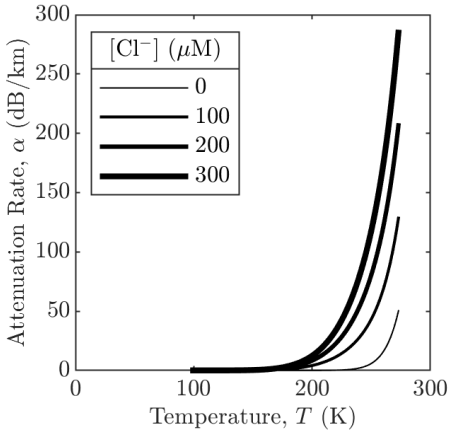

Figure 2. The simplified model of temperature and chemistry-dependent englacial radar attenuation rates considered in this work. Following Souček et al. (2023) and Moore (2000), we assume attenuation is dominated by a single impurity, chloride. This allows us to illustrate the effect of ice impurity for attenuation-based constraints on D_{cond} in terms of a single impurity parameter [Cl^-], defined as the concentration of chloride in the ice lattice in units of µM. We consider a range of chlorinity spanning from pure ice (0 µM) to chloride-saturated ice (300 µM) (Stillman et al., 2013).

3 Results

Using the illustrative forward models in Section 2, we consider the detection of two cases of potential subsurface radar signatures—thermally diagnostic interfaces (e.g., pore-curing and eutectic melt) and an isolated unattributed interface—and show the reduction in the subset of observation-compatible thermal profiles (and corresponding conductive-layer thicknesses). We assume an echo depth uncertainty of 150 m for eutectic melt, corresponding to the required range for REASON's HF band (Blankenship et al., 2024). For pore-curing we assume a higher echo depth uncertainty of 1 km to reflect the likely challenges in constraining the pore-curing depth given the expectation of slow changes in porosity with depth and the influence of volume clutter on the radar reflectivity.

3.1 Constraints from Isolated Unattributed Echoes

Isolated unattributed echoes are sparse echoes that cannot be attributed to a thermally diagnostic source. Although the only information these echoes provide is that "something" was detected at a given depth, the mere fact it was detected places an upper limit on the integrated two-way attenuation to the detection depth. Because the englacial attenuation rate of radar is dependent on temperature (e.g. Figure 2), this maximum two-way attenuation also places limits about the temperature profile above the detection depth (Matsuoka et al., 2012). For example, if we assume (for illustration) that a radar sounding link budget implies that no subsurface echo (even one from a perfectly reflecting subsurface interface beneath a perfectly transmitting surface) could be detected with more that 40 dB of attenuation, then the detection of "anything at all" means the integrated two-way attenuation to the detection depth must be less than 40 dB. Figure 3a shows this constraint for the case of pure ice. The implication of this result is the thermally conductive portion of the ice shell is at least as thick as the echo detection depth—in this case $D = 20.00 \pm 0.15$ km, thereby providing a lower limit for the layer thickness, $D_{\text{cond}} \geq$

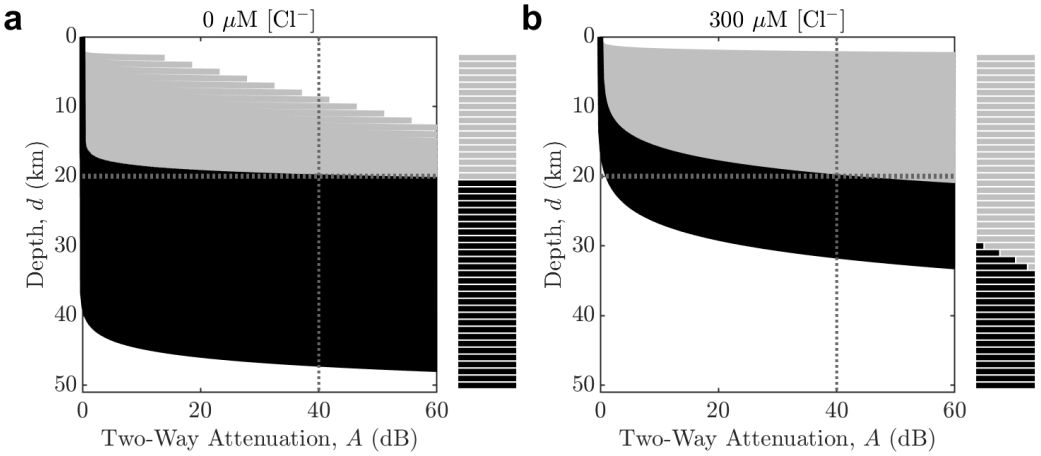

Figure 3. Attenuation–depth profiles for pure ice (a) and chloride-saturated ice (b). If a single subsurface radar echo is observed at depth $D = 20.00 \pm 0.15$ km, that observation alone (grey dashed line) sets a maximum two-way attenuation to that depth, which in turn provides a one-sided constraint the conductive layer thermal profile and thickness. The strength of this constraint depends on the whether the ice is pure (a) or on the concentration of conductivity-enhancing impurities (in our model assumed to be only chloride) (b).

D. Figure 3a also shows that the constraining power of unattributed echo detection for ice shells with higher impurities and attenuation rates is more powerful (though still provides only a lower limit). This is because the higher attenuation rate for impure ice (Figure 2) means that, for our example, echoes had to come from further up in the conductive portion of the ice shell to be detected. As a result, our thickness constraint for 300 µM ice shell is > 30 km rather than > 20 km for pure ice. This difference in Figure 3 also shows the improvement in the conductive thickness constraint that results from knowing the impurity chemistry of the shell, without which we'd be left with Figure 3a regardless of the true chemistry.

3.2 Constraints from Thermally Diagnostic Interfaces

The shallowest subsurface layer of Europa is thought to be a cold, porous, icy regolith (Daubar et al., 2024). While the presence of void space is unlikely to cause volume scattering losses sufficient to prevent the detection of deeper interfaces, volume scattering does have the potential to produce a detectable increase in background power (Eluszkiewicz, 2004; Aglyamov et al., 2017). This kind of signature has been observed for Earth's ice sheets, for example in UHF observations of the near-surface of the Greenland ice sheet, where it has been used to identify bodies of solid ice (with lower background power) emplaced within the porous firn layer (Culberg et al., 2021). As with Greenland firn, if the pores in Europa's regolith close, the corresponding drop in background power has the potential to provide an interpretable radar signature of the pore curing depth (or at least of the depth at which pores decrease below the size of detectability). In this work, we assume that within Europa's ice shell, ice begins to flow, allowing pores to close (or at least decrease in size) (Aglyamov et al., 2017). Following Howell (2021), we assume a porosity-curing temperature T_ϕ between 150 ± 20 K. Therefore, if radar-sounding profiles from REASON contain detectable background power from volume scattering that is attributed to regolith porosity that is also observed to drop in power as a result of pore curing, we can place a constraint on the ice shell temperature at the depth of that observation. This

temperature constraint, in turn, places limits on the range of observation-compatible thermal profiles and conductive layer thicknesses. For example, Figure 4a shows the impact of such an observation at depth $D = 5.00 \pm 0.15$ km attributed to ice-flow and pore-curing, therefore implying a temperature of 150 ± 20 K, and reducing the range of possible thermal profiles (grey) to an observation-compatible subset (black). As the histogram in Figure 4a shows, this corresponds to a reduction in possible conductive layer thickness, D_{cond} from $3 - 50$ km (grey) to $8 - 34$ km in this example.

Similarly, at depths within the ice shell that reach the liquidus of water-salt mixtures, melt can form, with the lowest temperatures for melting corresponding to the eutectic composition of salt-saturated brines (Wolfenbarger et al., 2022). This melt water has the potential to produce effective reflectivity values sufficient for detection in sounding records (Culha et al., 2020). Detection of eutectic melt is particularly aided by the lower attenuation rates due the relatively colder ice up to the depth where the eutectic temperature occurs (Kalousová et al., 2017). The temperature at which eutectic melt forms depends on the background chemistry of the ice (Wolfenbarger et al., 2022). For example, for ice containing NaCl, the eutectic temperature is approximately 252 K whereas for ice containing $MgSO_4$ the eutectic temperature is approximately 269 K (Wolfenbarger et al., 2022). For sea ice on Earth, which is composed of the same ionic species as seawater, the eutectic temperature is approximately 237 K (Wolfenbarger et al., 2022). Notably, this is the same eutectic temperature obtained by Zolotov and Shock (2001) for their model of a sulfate-dominated Europan ocean. As such, for this study we consider a eutectic temperature of 237 ± 1 K which could be representative of either a sulfate or chloride-dominated Europan ocean, which are often considered the end-member compositions for Europa's ocean (Wolfenbarger et al., 2022). Therefore, if REASON radar sounding profiles include echoes that can be attributed to eutectic melt, we can constrain the ice shell temperature at the depth of that observation. For example, Figure 4b shows how the observation of an echo at depth 20.00 ± 0.15 km attributed to eutectic melt implies a temperature of 237 ± 1 K at that depth, which reduces the possibilities (grey) to observation-compatible profiles (black). In this example, this corresponds to a reduction in possible conductive layer thicknesses from $3-50$ km (grey) to $23-24$ km (black).

In addition to the individual detection scenarios described above, it is promising to consider the detection of two or more thermally-diagnostic echoes. For example, we can consider the detection and interpretation of the same echo from pore-curing described above (e.g. Figure 4a) and the same echo from eutectic melt (e.g. Figure 4b). In this scenario, the combined constraint can improve the estimate of conductive ice shell thickness (as shown in Figure 4c) relative to either observation alone. In this example, those combined observations would reduce the possible thickness of D_{cond} from $3-50$ km (grey) to 24 km (black).

4 Discussion

In our illustrative results, thermally diagnostic signatures (i.e. pore-curing or eutectic melt) provided much stronger constraints than the attenuation-based constraint from mere detection of an unattributed echo. This is because the thermally diagnostic constraints make stronger assumptions and are directly connected to temperature profile and thickness of the conductive layer of the ice shell. These "two-sided" constraints are also stronger than the "one-sided" constraint placed by unattributed echoes (Figure 3). However, to enjoy this benefit, this also means that the source of these echoes must be interpreted or assumed to be coming from that particular feature. By contrast, the detection of an unattributed echo places coarser constraints on the temperature profile or thickness but also requires minimal assumptions or interpretation. Additionally, the strength of this one-sided constraint can be improved with additional knowledge or assumptions, such as those relating to the ice chemistry, surface transmission losses, the subsurface interface material and geometry, or radiometric calibration of the radar.

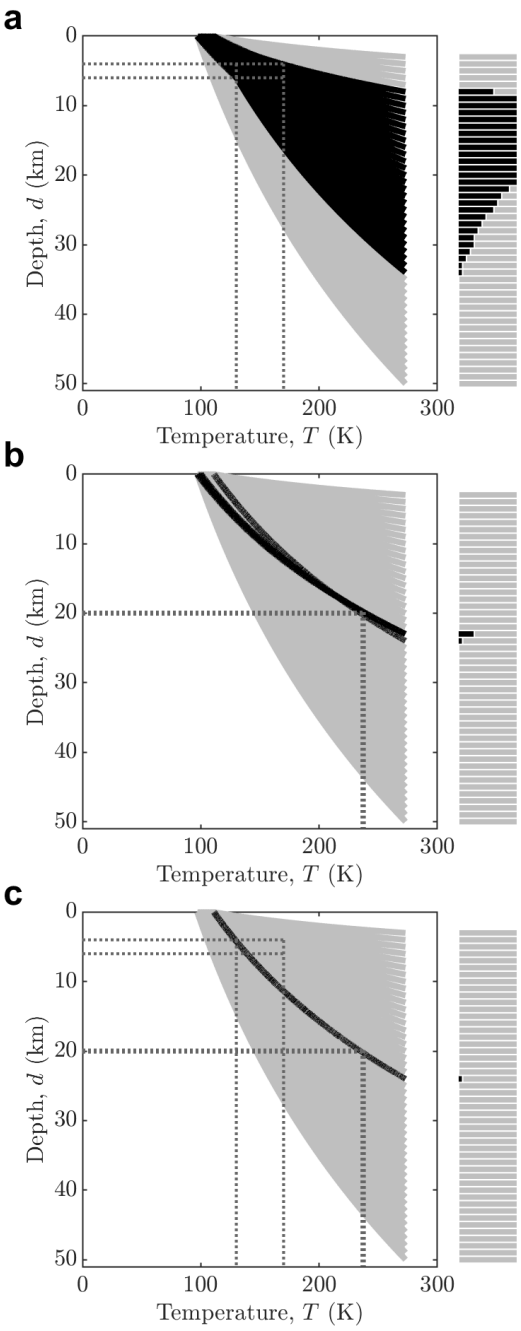

Figure 4. (a) If a radar signature attributed to pore curing (e.g. a drop in volume scattered power) is detected at depth $D = 5 \pm 1$ km (and therefore a temperature of 150 ± 20 K) this observation alone (grey dashed line) can constrain the range of potential conductive layer thermal profiles shown in the curves (left) and and thicknesses shown in the histogram (right) from the possible (grey) to the observation-compatible subset (black). (b) Similarly, if an echo in radar-sounding profiles attributed to eutectic melt (implying a temperature of 237 ± 1 K) is detected at depth $D = 20.00 \pm 0.15$ km, this observation alone (grey dashed line) can constrain also conductive layer thermal profile and thickness. (c) If both are detected (grey dashed lines), the combined constraint on the conductive layer thermal profile and thickness are better constrained than either feature alone.

Of the radar signatures we investigated, the detection and attribution of echoes from eutectic melt provided the strongest constraint on the conductive layer for two reasons: 1) eutectic melt had the narrowest range of associated diagnostic temperatures and 2) it occurred closer in temperature and depth to the base of the conductive layer (Howell, 2021; Kalousová et al., 2017). While this second factor will always be true, the first can (and likely will) evolve with additional modeling, observational, and experimental work investigating both pore-curing and eutectic processes in Europa-relevant ices (Kalousová et al., 2017; Wolfenbarger et al., 2022). This is perhaps the most significant result of our work: that improved understanding of the processes and conditions governing the formation and radar detectability of thermally-diagnostic signatures (e.g. pore-curing, eutectic melt) has the potential to improve the observational constraints on the conductive layer thickness of Europa's the ice shell from echoes shallower than the ice–ocean interface. Similarly, advances in the radio glaciological characterization and discrimination of these thermally diagnostic features (e.g. eutectic melt) from those of other water (e.g. impact melt or perched sills) or non-water (e.g. surface clutter, salt layers) features will be critical in moving these echoes from detection-based constraints (e.g. Figure 3) to far stronger attribution-based constraints (e.g. Figure 4b,c) (Schmidt et al., 2011; Castelletti et al., 2017; Steinbrügge et al., 2018; Culha et al., 2020; Culberg et al., 2021; Wolfenbarger et al., 2022)

Our results show that both pore-curing and eutectic echoes can place powerful constraints on the conductive layer thickness of the ice shell because they place both depth and temperature constraints. This raises the promising possibility to implement the strategy proposed by Kalousová et al. (2017) of characterizing the convective structure of Europa's ice shell by mapping these thermally diagnostic interfaces along longitudinal cross-sections. However, as shown in Figure 5, the colder temperature (and therefore shallower depth) of the pore-curing signature falls in the middle of the conductive layer and therefore does not express the shape of convecting cells to the same degree as eutectic echoes, which (at warmer temperatures and deeper depth) can encode rich information about the convective layer (e.g. the strength, number, and thickness of convective cells). As a result, eutectic echo mapping stands to be a powerful observational constraint for both the conductive shell (e.g. our result above) but also for constraining the convective portion of Europa's shell.

In our illustrative approach, we fixed the convective layer temperature at 273 K, which results in a maximum estimate for two-way attenuation to a given depth within the ice shell. In practice, the temperature at which ice can remain thermodynamically stable decreases with increasing ice thickness to a temperature of approximately 268 K beneath 50 km of ice at Europa. The temperature of the convective layer predicted by convection models is sensitive to assumptions about the ice rheology, ranging from 235 K to the pressure-dependent melting temperature (Pappalardo et al., 1998; Kalousová et al., 2017). Howell (2021) consider a convective layer temperature range of $251.60^{+0.37}_{-1.10}$ K. For colder convective layer temperatures, the position of the thermally diagnostic interfaces within the conductive ice layer will move closer to the base of the conductive layer. For convective layer temperatures above the eutectic temperature, this implies that eutectic melt would exist within the convective layer itself. For our assumed eutectic temperature (237 K), the eutectic melt would be in the convective layer only for the lower bound estimates of convective layer temperature. Generally the principles introduced in this work will hold for lower convective temperatures and the associated radar signatures are likely to be even stronger and more thermally diagnostic. With improved understanding of the stability and character of these thermally diagnostic interfaces, the approach presented in this work could place tighter constraints on the thickness and thermophysical properties of Europa's ice shell.

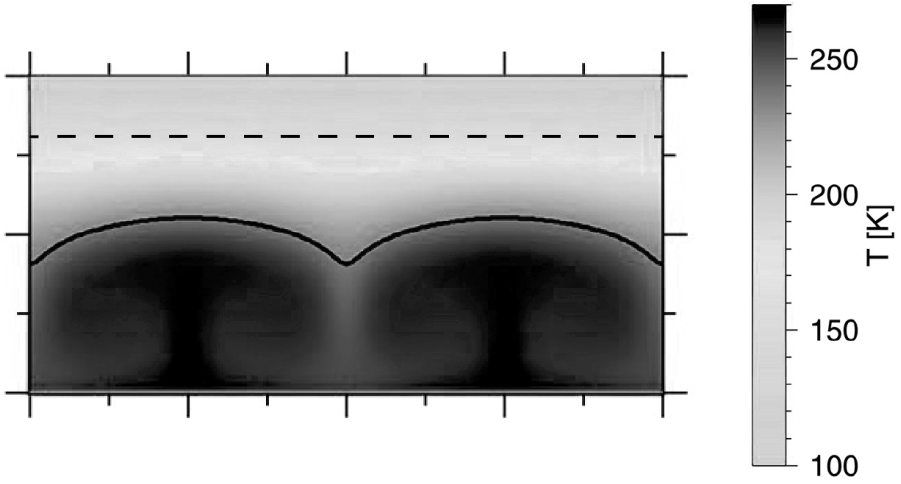

Figure 5. One longitudinal cross section of ice shell temperatures adapted from Kalousová et al. (2017) showing that eutectic isotherms (solid black line) express the configuration of the underlying convective layer more than pore-curing isotherms (dashed black line).

5 Conclusions

Taken as a whole, our results show that radar signatures other than direct detection of the ice–ocean interface can help constrain the thermophysical configuration of Europa's ice shell, including the thermal profile within and the thickness of the conductive portion of its ice shell. This kind of constraint on the conductive portion of the ice shell is powerful in the context of complementary observational constraints on the total ice shell thickness. For example, if these radar signatures are detected in concert with direct ice–ocean echoes, the combination of these echoes can dramatically improve the constraints on the entire ice temperature profile (Blankenship et al., 2024). Similarly, if constraints on total ice shell thickness are provided by gravity/tides, magnetometer data, or global shape (Steinbrügge et al., 2018; Kivelson et al., 2023; Mazarico et al., 2023b) then these additional observations can also improve our joint constraints on ice shell thermal profiles (e.g. convection). In each of these cases, the combination of observations has the potential to decrease the degeneracy/ambiguity in any one observation alone, such as the ambiguity in ice shell thickness and ocean salinity from a magnetometer alone (Kivelson et al., 2000, 2023) or the combination of rheology and thickness for gravity alone (Steinbrügge et al., 2018; Mazarico et al., 2023b). In addition to these more straightforward opportunities for multi-observation synthesis, these signatures also have the potential to be combined with surface reflectometry (Grima et al., 2014; Blankenship et al., 2024), radiometer data (Janssen et al., 2017), or thermal imaging to constrain near-surface porosity and shallow subsurface processes and conditions (Culberg et al., 2021; Steinbrügge et al., 2020). These results invite us to expand our imagination of what radar sounding observations beyond direct detection of the ice–ocean interface may mean for Europa interior science (Roberts et al., 2023). Our results also provide motivation for further investigation into ice–water processes, radar signatures, and data analysis for pore curing and eutectic melt in Europa's ice shell. When integrated into a larger joint geophysical investigation of the Europan interior, these observations (in addition to any direct ice–ocean interface detection) stand to dramatically increase our understanding of Europa's ice shell from the ocean to the near-surface (Blankenship et al., 2024).

6 Open Research

No data has been used or generated as part of this publication. The results presented are entirely analytical and fully described by the equations within the manuscript.

Acknowledgments
The research was carried out, in part, at the Jet Propulsion Laboratory, California Institute of Technology, under a contract with the National Aeronautics and Space Administration (80NM0018D0004) and funded by the Europa Clipper project.

References

Aglyamov, Y., Schroeder, D. M., & Vance, S. D. (2017). Bright prospects for radar detection of Europa's ocean. *Icarus*, *281*, 334–337. doi: 10.1016/j.icarus.2016.08.014

Becker, T., Zolatov, M., Yu, M., Gudipati, M., Soderblom, J., McGrath, M., ... others (2024). Exploring the composition of europa with the upcoming europa clipper mission. *Space Science Reviews*, *220*(1).

Billings, S. E., & Kattenhorn, S. A. (2005). The great thickness debate: Ice shell thickness models for europa and comparisons with estimates based on flexure at ridges. *Icarus*, *177*(2), 397–412.

Blankenship, D., Moussessian, A., Chapin, E., Young, D., Patterson, G., Plaut, J., ... others (2024). Radar for europa assessment and sounding: Ocean to near-surface (reason). *Space Science Reviews*, *220*(1). doi: https://doi.org/10.1007/s11214-024-01072-3

Castelletti, D., Schroeder, D. M., Hensley, S., Grima, C., Ng, G., Young, D., ... Blankenship, D. D. (2017). An Interferometric Approach to Cross-Track Clutter Detection in Two-Channel VHF Radar Sounders. *IEEE Transactions on Geoscience and Remote Sensing*, *55*(11), 6128–6140. doi: 10.1109/tgrs.2017.2721433

Chyba, C. F., Ostro, S. J., & Edwards, B. C. (1998). Radar Detectability of a Subsurface Ocean on Europa. *Icarus*, *134*(2), 292–302. doi: 10.1006/icar.1998.5961

Culberg, R., Schroeder, D. M., & Steinbrügge, G. (2021). Double ridge formation over shallow water sills on Jupiter's moon Europa. *Nature communications*, *13*(1), 2007. doi: 10.1038/s41467-022-29458-3

Culha, C., Schroeder, D. M., Jordan, T. M., & Haynes, M. S. (2020). Assessing the detectability of Europa's eutectic zone using radar sounding. *Icarus*, *339*, 113578. doi: 10.1016/j.icarus.2019.113578

Daubar, I. J., Hayes, A. G., Collins, G. C., Craft, K. L., Rathbun, J. A., Spencer, J. R., ... Pappalardo, R. (2024). Planned Geological Investigations of the Europa Clipper Mission. *Space Science Reviews*, *220*(1), 18. doi: 10.1007/s11214-023-01036-z

Eluszkiewicz, J. (2004). Dim prospects for radar detection of Europa's ocean. *Icarus*, *170*(1), 234–236. doi: 10.1016/j.icarus.2004.02.011

Grima, C., Schroeder, D. M., Blankenship, D. D., & Young, D. A. (2014). Planetary landing-zone reconnaissance using ice-penetrating radar data: Concept validation in Antarctica. *Planetary and Space Science*, *103*, 191–204. doi: 10.1016/j.pss.2014.07.018

Howell, S. M. (2021). The Likely Thickness of Europa's Icy Shell. *The Planetary Science Journal*, *2*(4), 129. doi: 10.3847/psj/abfe10

Janssen, M. A., Oswald, J. E., Brown, S. T., Gulkis, S., Levin, S. M., Bolton, S. J., ... Wang, C. C. (2017). MWR: Microwave Radiometer for the Juno Mission to Jupiter. *Space Science Reviews*, *213*(1-4), 139–185. doi: 10.1007/s11214-017-0349-5

Johnson, B. C., Sheppard, R. Y., Pascuzzo, A. C., Fisher, E. A., & Wiggins, S. E. (2017). Porosity and salt content determine if subduction can occur in europa's ice shell. *Journal of Geophysical Research: Planets*, *122*(12), 2765-2778. Retrieved from https://agupubs.onlinelibrary.wiley.com/doi/abs/10.1002/2017JE005370 doi: https://doi.org/10.1002/2017JE005370

Kalousová, K., Schroeder, D. M., & Soderlund, K. M. (2017). Radar attenuation in Europa's ice shell: Obstacles and opportunities for constraining the shell thickness and its thermal structure. *Journal of Geophysical Research: Planets*, *122*(3), 524–545. doi: 10.1002/2016je005110

Kivelson, M. G., Jia, X., Lee, K. A., Raymond, C. A., Khurana, K. K., Perley, M. O., ... Wigglesworth, L. (2023). The Europa Clipper Magnetometer. *Space Science Reviews*, *219*(6), 48. doi: 10.1007/s11214-023-00989-5

Kivelson, M. G., Khurana, K. K., Russell, C. T., Volwerk, M., Walker, R. J., & Zimmer, C. (2000). Galileo Magnetometer Measurements: A Stronger Case for a Subsurface Ocean at Europa. *Science*, *289*(5483), 1340–1343. doi: 10.1126/science.289.5483.1340

MacGregor, J. A., Li, J., Paden, J. D., Catania, G. A., Clow, G. D., Fahnestock, M. A., ... Stillman, D. E. (2015, 6). Radar attenuation and temperature within the Greenland Ice Sheet. *Journal of Geophysical Research: Earth Surface*, *120*(6), 983–1008. doi: 10.1002/2014jf003418

MacGregor, J. A., Winebrenner, D. P., Conway, H., Matsuoka, K., Mayewski, P. A., & Clow, G. D. (2007). Modeling englacial radar attenuation at siple dome, west antarctica, using ice chemistry and temperature data. *Journal of Geophysical Research: Earth Surface*, *112*(F3). Retrieved from https://agupubs.onlinelibrary.wiley.com/doi/abs/10.1029/2006JF000717 doi: https://doi.org/10.1029/2006JF000717

Matsuoka, K., MacGregor, J. A., & Pattyn, F. (2012). Predicting radar attenuation within the Antarctic ice sheet. *Earth and Planetary Science Letters*, *359*, 173–183. doi: 10.1016/j.epsl.2012.10.018

Mazarico, E., Buccino, D., Castillo-Rogez, J., Dombard, A. J., Genova, A., Hussmann, H., ... others (2023a). The europa clipper gravity and radio science investigation. *Space Science Reviews*, *219*(4), 30.

Mazarico, E., Buccino, D., Castillo-Rogez, J., Dombard, A. J., Genova, A., Hussmann, H., ... Withers, P. (2023b). The Europa Clipper Gravity and Radio Science Investigation. *Space Science Reviews*, *219*(4), 30. doi: 10.1007/s11214-023-00972-0

Moore, J. C. (2000). Models of radar absorption in europan ice. *Icarus*, *147*(1), 292-300. Retrieved from https://www.sciencedirect.com/science/article/pii/S001910350096425X doi: https://doi.org/10.1006/icar.2000.6425

Nimmo, F., Pappalardo, R., & Giese, B. (2003). On the origins of band topography, europa. *Icarus*, *166*(1), 21-32. Retrieved from https://www.sciencedirect.com/science/article/pii/S0019103503002367 doi: https://doi.org/10.1016/j.icarus.2003.08.002

Pappalardo, R., Buratti, B., Korth, H., Senske, D., Blaney, D., Blankenship, D., ... others (2024). Science overview of the europa clipper mission. *Space Science Reviews*, *220*(1).

Pappalardo, R., Head, J., Greeley, R., Sullivan, R., Pilcher, C., Schubert, G., ... others (1998). Geological evidence for solid-state convection in europa's ice shell. *Nature*, *391*(6665), 365–368.

Roberts, J. H., McKinnon, W. B., Elder, C. M., Tobie, G., Biersteker, J. B., Young, D., ... Group, I. T. W. (2023). Exploring the Interior of Europa with the Europa Clipper. *Space science reviews*, *219*(6), 46. doi: 10.1007/s11214-023-00990-y

Schmidt, B. E., Blankenship, D. D., Patterson, G. W., & Schenk, P. M. (2011). Active formation of 'chaos terrain' over shallow subsurface water on Europa. *Na-*

ture, *479*(7374), 502–5. doi: 10.1038/nature10608

Souček, O., Běhounková, M., Schroeder, D. M., Wolfenbarger, N. S., Kalousová, K., Steinbrügge, G., & Soderlund, K. M. (2023). Radar Attenuation in Enceladus' Ice Shell: Obstacles and Opportunities for Constraining Shell Thickness, Chemistry, and Thermal Structure. *Journal of Geophysical Research: Planets*, *128*(2). doi: 10.1029/2022je007626

Steinbrügge, G., Schroeder, D., Haynes, M., Hussmann, H., Grima, C., & Blankenship, D. (2018). Assessing the potential for measuring Europa's tidal Love number h 2 using radar sounder and topographic imager data. *Earth and Planetary Science Letters*, *482*, 334–341. doi: 10.1016/j.epsl.2017.11.028

Steinbrügge, G., Voigt, J. R. C., Wolfenbarger, N. S., Hamilton, C. W., Soderlund, K. M., Young, D. A., ... Schroeder, D. M. (2020). Brine Migration and Impact-Induced Cryovolcanism on Europa. *Geophysical Research Letters*, *47*(21). doi: 10.1029/2020gl090797

Stillman, D. E., Macgregor, J. A., & Grimm, R. E. (2013). Electrical response of ammonium-rich water ice. *Annals of Glaciology*, *54*(64), 21–26. doi: 10.3189/2013AoG64A204

Vance, S. D., Craft, K. L., Shock, E., Schmidt, B. E., Lunine, J., Hand, K. P., ... Elder, C. M. (2023). Investigating Europa's Habitability with the Europa Clipper. *Space Science Reviews*, *219*(8), 81. doi: 10.1007/s11214-023-01025-2

Wolfenbarger, N. S., Fox-Powell, M. G., Buffo, J. J., Soderlund, K. M., & Blankenship, D. D. (2022). Compositional Controls on the Distribution of Brine in Europa's Ice Shell. *Journal of Geophysical Research: Planets*, *127*(9). doi: 10.1029/2022je007305

Zolotov, M. Y., & Shock, E. L. (2001). Composition and stability of salts on the surface of europa and their oceanic origin. *Journal of Geophysical Research: Planets*, *106*(E12), 32815-32827. Retrieved from `https://agupubs.onlinelibrary.wiley.com/doi/abs/10.1029/2000JE001413` doi: https://doi.org/10.1029/2000JE001413